Short Papers

Maximum Likelihood Estimation Methods for Multispectral Random Field Image Models

Jesse Bennett, *Member*, *IEEE*, and
Alireza Khotanzad, *Member*, *IEEE*

Abstract—This work considers the problem of estimating parameters of multispectral random field (RF) image models using maximum likelihood (ML) methods. For images with an assumed Gaussian distribution, analytical results are developed for multispectral simultaneous autoregressive (MSAR) and Markov random field (MMRF) models which lead to practical procedures for calculating ML estimates. Although previous work has provided least squares methods for parameter estimation, the superiority of the ML method is evidenced by experimental results provided in this work. The effectiveness of multispectral RF models using ML estimates in modeling color texture images is also demonstrated.

Index Terms—Maximum likelihood estimation, multispectral image models, color texture models, multispectral random fields, multispectral autoregressive models, multispectral Markov models.

1 Introduction

With recent advances in imaging technology there is an increasing need for analysis methods suited to multispectral images, particularly the subclass of color images. Previous methods typically involve mapping color to gray tones [1], which allows the use of existing gray tone models. Although the simplicity of this approach is attractive, the resulting models suffer considerable loss of image information. One statistical image model that is particularly well suited to analysis of color image texture is the multispectral random field model considered in this work.

The class of random field (RF) models based on intensity images has been widely used in many application areas, including image synthesis and analysis [2], [3], image compression [4], geodesy [5], and agriculture [6], [7]. To date, however, there has been little work in the area of modeling color images using these methods. A method for image segmentation based on color RF models can be found in [8]. A more complete treatment of these models is given in [9], [10]. In this work, maximum likelihood (ML) methods for estimating multispectral RF model parameters are considered. Experimental results demonstrate the superiority of ML estimates over those obtained using least squares (LS) methods.

Two frequently used RF models are the Simultaneous autoregressive (SAR) and Markov random field (MRF) models considered here. In the multispectral case, these models are defined as intensity levels on multiple two-dimensional lattice planes, with the intensity level at each lattice location taken to be a linear combination of neighboring intensity levels and an additive noise sample. For a multispectral image with P intensity planes, these models are characterized by P^2 sets of relative neighbor locations and neighbor coefficients.

For mathematical simplicity, the models considered here are formulated using the toroidal lattice assumption [11]. A location within an $M \times M$ two-dimensional lattice is denoted by $\mathbf{s} = (s_1, s_2)$, with s_1, s_2 integers from the set $J = \{0, 1, ..., M-1\}$. The set of all lattice locations is defined as $\Omega = \{\mathbf{s} = (s_1, s_2) : s_1, s_2 \in J\}$. The value of an image observation at location $\mathbf{s}$ is denoted by the vector value $\mathbf{y}(\mathbf{s})$, and the image observations are assumed to have zero mean.

Neighbor sets relating the dependence of image plane i on image plane j are defined as $N_{ij} = \{\mathbf{r} = (k, l) : k, l \in \pm J\}$, with the associated neighbor coefficients given by $\boldsymbol{\theta}_{ij} = \{\theta_{ij}(\mathbf{r}) : \mathbf{r} \in N_{ij}\}$. Neighbor sets may be classified as *symmetric* or *nonsymmetric*. In the case of multispectral models, a symmetric neighbor set is defined as one for which $\mathbf{r} \in N_{ij} \Leftrightarrow -\mathbf{r} \in N_{ji}$. In addition, for each image plane there is a scale parameter ρ_i associated with the corresponding noise component of the model. Model parameters will be referred to collectively as $\boldsymbol{\theta} = \{\boldsymbol{\theta}_{ij};\ i, j \in \{1, \ldots, P\}\}$ and $\boldsymbol{\rho} = \{\rho_i;\ i \in \{1, \ldots, P\}\}$.

2 Multispectral Simultaneous Autoregressive (MSAR) Models

The multispectral SAR (MSAR) model relates the observations at each lattice location to its neighbors, both within and between image planes, according to the model equations

$$y_i(\mathbf{s}) = \sum_{j=1}^{P} \sum_{\mathbf{r} \in N_{ij}} \theta_{ij}(\mathbf{r}) y_j(\mathbf{s} \oplus \mathbf{r}) + \sqrt{\rho_i}\, w_i(\mathbf{s}),$$
$$\mathbf{s} \in \Omega \text{ and } i = 1, \ldots, P \tag{1}$$

where

P = number of image planes
N_{ij} = neighbor set relating pixels in plane i to neighbors in plane j (only interplane neighbor sets, i.e., $N_{ij,\, i \neq j}$, may include the (0,0) neighbor)
$\boldsymbol{\theta}_{ij}$ = coefficients which define the dependence of $y_i(\mathbf{s})$ on its neighbor set N_{ij}
ρ_i = noise variance of image plane i
$w_i(\mathbf{s})$ = i.i.d. random variables with zero mean and unit variance

and $\oplus$ denotes modulo M addition in each index. The MSAR model characterizes spatial interactions between neighboring pixels through the parameter vectors $\boldsymbol{\theta}$ and $\boldsymbol{\rho}$.

Rewriting (1) in matrix form, the MSAR model equations are given by

$$\mathbf{B}(\boldsymbol{\theta})\mathbf{y} = \mathbf{w}$$

where

$$\mathbf{B}(\theta) = \begin{bmatrix} \mathbf{B}(\boldsymbol{\theta}_{11}) & \mathbf{B}(\boldsymbol{\theta}_{12}) & \cdots & \mathbf{B}(\boldsymbol{\theta}_{1P}) \\ \mathbf{B}(\boldsymbol{\theta}_{21}) & \mathbf{B}(\boldsymbol{\theta}_{22}) & \cdots & \mathbf{B}(\boldsymbol{\theta}_{2P}) \\ \vdots & \vdots & \ddots & \vdots \\ \mathbf{B}(\boldsymbol{\theta}_{P1}) & \mathbf{B}(\boldsymbol{\theta}_{P2}) & \cdots & \mathbf{B}(\boldsymbol{\theta}_{PP}) \end{bmatrix},$$
$$\text{a } PM^2 \times PM^2 \text{ matrix} \tag{3}$$

$$\mathbf{y} = \begin{bmatrix} \mathbf{y}_1^T & \mathbf{y}_2^T & \cdots & \mathbf{y}_P^T \end{bmatrix}^T, \text{ a } PM^2 \times 1 \text{ vector}$$

• *The authors are with the Department of Electrical Engineering, Southern Methodist University, Dallas, TX 75275-0338 USA. E-mail: kha@seas.smu.edu; jesse.bennett@ieee.org.*

Manuscript received 28 Apr. 1997; revised 7 Oct. 1998. Recommended for acceptance by R. Picard.
For information on obtaining reprints of this article, please send e-mail to: tpami@computer.org, and reference IEEECS Log Number 108017.

$$\mathbf{w} = \left[\sqrt{\rho_1}\mathbf{w}_1^T \quad \sqrt{\rho_2}\mathbf{w}_2^T \quad \cdots \quad \sqrt{\rho_P}\mathbf{w}_P^T\right]^T, \text{ a } PM^2 \times 1 \text{ vector}$$

and $\mathbf{y}_i$ and $\mathbf{w}_i$ are $M^2 \times 1$ vectors of lexicographic ordered arrays $\{y_i(\mathbf{s})\}$ and $\{w_i(\mathbf{s})\}$, respectively. The transformation matrix $\mathbf{B}(\boldsymbol{\theta})$ is composed of $M^2 \times M^2$ block-circulant submatrices

$$\mathbf{B}\left(\boldsymbol{\theta}_{ij}\right) = \begin{bmatrix} \mathbf{B}\left(\boldsymbol{\theta}_{ij}\right)_1 & \mathbf{B}\left(\boldsymbol{\theta}_{ij}\right)_2 & \cdots & \mathbf{B}\left(\boldsymbol{\theta}_{ij}\right)_M \\ \mathbf{B}\left(\boldsymbol{\theta}_{ij}\right)_M & \mathbf{B}\left(\boldsymbol{\theta}_{ij}\right)_1 & \cdots & \mathbf{B}\left(\boldsymbol{\theta}_{ij}\right)_{(M-1)} \\ \vdots & \vdots & \ddots & \vdots \\ \mathbf{B}\left(\boldsymbol{\theta}_{ij}\right)_2 & \mathbf{B}\left(\boldsymbol{\theta}_{ij}\right)_3 & \cdots & \mathbf{B}\left(\boldsymbol{\theta}_{ij}\right)_1 \end{bmatrix} \tag{4}$$

where each $\mathbf{B}(\boldsymbol{\theta}_{ij})_p$ is an $M \times M$ circulant matrix whose (m, n)th element is given by [12]:

$$b\left(\boldsymbol{\theta}_{ij}\right)_p(m,n) = \begin{cases} 1 & i = j, p = 1 \text{ and } m = n \\ -\theta_{ij}(k,l) & k = p-1, l = \left((n-m) \bmod M\right) \text{ and } (k,l) \in N_{ij} \\ 0 & \text{otherwise} \end{cases} \tag{5}$$

A sufficient condition for the MSAR model to exist and be stable is that $\mathbf{B}(\boldsymbol{\theta})$ be nonsingular or, equivalently, $|\mathbf{B}(\boldsymbol{\theta})| \neq 0$.

Writing the image observations as $\mathbf{y} = \mathbf{B}(\boldsymbol{\theta})^{-1}\mathbf{w}$, the image covariance matrix is obtained as

$$\Sigma_{\mathbf{y}} = E\left\{\mathbf{y}\mathbf{y}^T\right\} = E\left\{\mathbf{B}(\boldsymbol{\theta})^{-1}\mathbf{w}\mathbf{w}^T\left[\mathbf{B}(\boldsymbol{\theta})^{-1}\right]^T\right\} = \mathbf{B}(\boldsymbol{\theta})^{-1}\Sigma_{\mathbf{w}}\left[\mathbf{B}(\boldsymbol{\theta})^{-1}\right]^T \tag{6}$$

where

$$\Sigma_{\mathbf{w}} = E\left\{\mathbf{w}\mathbf{w}^T\right\} = \begin{bmatrix} \rho_1\mathbf{I} & \mathbf{0} & \cdots & \mathbf{0} \\ \mathbf{0} & \rho_2\mathbf{I} & \cdots & \mathbf{0} \\ \vdots & \vdots & \ddots & \vdots \\ \mathbf{0} & \mathbf{0} & \cdots & \rho_P\mathbf{I} \end{bmatrix} \tag{7}$$

and $\mathbf{I}$ is the $M^2 \times M^2$ identity matrix. Due to the form of (6), the positive definite property required of $\Sigma_{\mathbf{y}}$ is ensured if $\mathbf{B}(\boldsymbol{\theta})$ is nonsingular.

Further details of the MSAR model, including methods for image synthesis and least squares parameter estimation, can be found in [9], [10], [12].

2.1 Maximum Likelihood Estimation of MSAR Model Parameters

If the image observations $\{\mathbf{y}(\mathbf{s})\}$ are assumed to have the multivariate Gaussian distribution

$$p\left(\mathbf{y}|\boldsymbol{\theta}, \rho\right) = \frac{1}{(2\pi)^{\frac{PM^2}{2}}\left|\Sigma_{\mathbf{y}}\right|^{\frac{1}{2}}} \exp\left\{-\frac{1}{2}\mathbf{y}^T\Sigma_{\mathbf{y}}^{-1}\mathbf{y}\right\} \tag{8}$$

then the log-likelihood of the observations can be written as

$$\log p\left(\mathbf{y}|\boldsymbol{\theta}, \boldsymbol{\rho}\right) = \frac{1}{2}\log\left|\Sigma_{\mathbf{y}}^{-1}\right| - \frac{PM^2}{2}\log 2\pi - \frac{1}{2}\mathbf{y}^T\Sigma_{\mathbf{y}}^{-1}\mathbf{y}. \tag{9}$$

The maximum likelihood parameter estimates are obtained by maximizing (9), which is equivalent to *minimizing*

$$J\left(\boldsymbol{\theta}, \boldsymbol{\rho}\right) = \mathbf{y}^T\Sigma_{\mathbf{y}}^{-1}\mathbf{y} - \log\left|\Sigma_{\mathbf{y}}^{-1}\right|. \tag{10}$$

From (6), using the identity $(\mathbf{CDE})^{-1} = \mathbf{E}^{-1}\mathbf{D}^{-1}\mathbf{C}^{-1}$, $\Sigma_{\mathbf{y}}^{-1}$ can be written as

$$\Sigma_{\mathbf{y}}^{-1} = \mathbf{B}(\theta)^T\Sigma_{\mathbf{w}}^{-1}\mathbf{B}(\theta) = \left(\Sigma_{\mathbf{w}}^{-\frac{1}{2}}\mathbf{B}(\theta)\right)^T\left(\Sigma_{\mathbf{w}}^{-\frac{1}{2}}\mathbf{B}(\theta)\right). \tag{11}$$

Substituting (11) for $\Sigma_{\mathbf{y}}^{-1}$ in the quadratic term of (10) yields

$$\mathbf{y}^T\Sigma_{\mathbf{y}}^{-1}\mathbf{y} = \mathbf{y}^T\left(\Sigma_{\mathbf{w}}^{-\frac{1}{2}}\mathbf{B}(\boldsymbol{\theta})\right)^T\left(\Sigma_{\mathbf{w}}^{-\frac{1}{2}}\mathbf{B}(\boldsymbol{\theta})\right)\mathbf{y} = \left(\Sigma_{\mathbf{w}}^{-\frac{1}{2}}\mathbf{B}(\boldsymbol{\theta})\mathbf{y}\right)^T\left(\Sigma_{\mathbf{w}}^{-\frac{1}{2}}\mathbf{B}(\boldsymbol{\theta})\mathbf{y}\right) = \left\|\Sigma_{\mathbf{w}}^{-\frac{1}{2}}\mathbf{B}(\boldsymbol{\theta})\mathbf{y}\right\|^2 \tag{12}$$

where $\|\cdot\|$ denotes the vector 2-norm. Now consider that the $PM^2 \times 1$ vector $\Sigma_{\mathbf{w}}^{-\frac{1}{2}}\mathbf{B}(\boldsymbol{\theta})\mathbf{y}$ can be written as

$$\Sigma_{\mathbf{w}}^{-\frac{1}{2}}\mathbf{B}(\boldsymbol{\theta})\mathbf{y} = \text{col}\left\{\frac{1}{\sqrt{\rho_i}}\sum_{j=1}^{P}\mathbf{B}\left(\boldsymbol{\theta}_{ij}\right)\mathbf{y}_j : i = 1, \ldots, P\right\}. \tag{13}$$

Using the identities

$$\left\|\left[\mathbf{a}_1^T \ \ldots \ \mathbf{a}_N^T\right]^T\right\| = \Sigma_i\|\mathbf{a}_i\|^2$$

and

$$\|\beta\mathbf{a}\|^2 = \beta^2\|\mathbf{a}\|^2$$

$$\left\|\Sigma_{\mathbf{w}}^{-\frac{1}{2}}\mathbf{B}(\boldsymbol{\theta})\mathbf{y}\right\|^2 = \sum_{i=1}^{P}\left\|\frac{1}{\sqrt{\rho_i}}\sum_{j=1}^{P}\mathbf{B}\left(\boldsymbol{\theta}_{ij}\right)\mathbf{y}_j\right\|^2 = \sum_{i=1}^{P}\frac{1}{\rho_i}\left\|\sum_{j=1}^{P}\mathbf{B}\left(\boldsymbol{\theta}_{ij}\right)\mathbf{y}_j\right\|^2. \tag{14}$$

Finally, noting that

$$\mathbf{B}\left(\boldsymbol{\theta}_{ij}\right)\mathbf{y}_j = \text{col}\left\{\delta_{ij}y_i(\mathbf{s}) - \sum_{\mathbf{r}\in N_{ij}}\theta_{ij}(\mathbf{r})y_j(\mathbf{s}\oplus\mathbf{r}) : \mathbf{s} \in \Omega\right\} \tag{15}$$

where δ_{ij} is the Kronecker delta function, (12) simplifies to

$$\mathbf{y}^T\Sigma_{\mathbf{y}}^{-1}\mathbf{y} = \sum_{i=1}^{P}\frac{1}{\rho_i}\sum_{\mathbf{s}\in\Omega}\left(\sum_{j=1}^{P}\left(\delta_{ij}y_i(\mathbf{s}) - \sum_{\mathbf{r}\in N_{ij}}\theta_{ij}(\mathbf{r})y_j(\mathbf{s}\oplus\mathbf{r})\right)\right)^2 = \sum_{i=1}^{P}\frac{1}{\rho_i}\sum_{\mathbf{s}\in\Omega}\left(y_i(\mathbf{s}) - \sum_{j=1}^{P}\sum_{\mathbf{r}\in N_{ij}}\theta_{ij}(\mathbf{r})y_j(\mathbf{s}\oplus\mathbf{r})\right)^2 \tag{16}$$

Using (11), the determinant in (10) can be expressed as

$$\left|\Sigma_{\mathbf{y}}^{-1}\right| = \left|\Sigma_{\mathbf{w}}^{-\frac{1}{2}}\mathbf{B}(\boldsymbol{\theta})\right|^2 = \left|\Sigma_{\mathbf{w}}\right|^{-1}\left|\mathbf{B}(\boldsymbol{\theta})\right|^2 = \left(\prod_{i=1}^{P}\rho_i\right)^{-M^2}\left|\mathbf{B}(\theta)\right|^2. \tag{17}$$

Theorem 1 is useful in simplifying the above expression.

THEOREM 1. *Let*

$$\mathbf{A} = \begin{bmatrix} \mathbf{A}_{11} & \mathbf{A}_{12} & \cdots & \mathbf{A}_{1Q} \\ \mathbf{A}_{21} & \mathbf{A}_{22} & \cdots & \mathbf{A}_{2Q} \\ \vdots & \vdots & \ddots & \vdots \\ \mathbf{A}_{Q1} & \mathbf{A}_{Q2} & \cdots & \mathbf{A}_{QQ} \end{bmatrix}, \tag{18}$$

where $\mathbf{A}$ *consists of* Q^2 *block-circulant submatrices* $\mathbf{A}_{ij}$ *with dimension* R. *Define* $\mathbf{U}$ *as the unitary matrix such that*

$$\mathbf{U}^H\mathbf{A}_{ij}\mathbf{U} = \mathbf{D}_{ij} = \text{diag}\{\lambda_{ij}(1), \ldots, \lambda_{ij}(R)\},$$

i.e., the diagonal elements of $\mathbf{D}_{ij}$ *are the eigenvalues of* $\mathbf{A}_{ij}$. *The existence of* $\mathbf{U}$ *is assured by the block-circulant structure of* $\mathbf{A}_{ij}$. *Then the eigenvalues of* $\mathbf{A}$,

$$\{\lambda(l) : l = 1, \ldots, QR\},$$

are equal to the eigenvalues of

$$\Lambda(n), \ n = 1, \ldots, R$$

where

$$\Lambda(n) = \begin{bmatrix} \lambda_{11}(n) & \lambda_{12}(n) & \cdots & \lambda_{1Q}(n) \\ \lambda_{21}(n) & \lambda_{22}(n) & \cdots & \lambda_{2Q}(n) \\ \vdots & \vdots & \ddots & \vdots \\ \lambda_{Q1}(n) & \lambda_{Q2}(n) & \cdots & \lambda_{QQ}(n) \end{bmatrix}. \tag{19}$$

In other words, $\lambda(1)$, …, $\lambda(Q)$ can be found as the eigenvalues of $\Lambda(1)$, $\lambda(Q+1)$, …, $\lambda(2Q)$ as the eigenvalues of $\Lambda(2)$, etc.

COROLLARY 1. $|\mathbf{A}| = \prod_{n=1}^{R} |\Lambda(n)|$.

PROOF. The $\mathbf{A}_{ij}$s are simultaneously diagonalized by the similarity transform $\mathbf{F}^H\mathbf{A}\mathbf{F} = \mathbf{D}$, where $\mathbf{F} = \text{diag}\{\mathbf{U}, \ldots, \mathbf{U}\}$. A simple permutation interchanging rows and columns transforms $\mathbf{D}$ to block diagonal form with diagonal blocks given by (19). Since the eigenvalues of a block diagonal matrix are the eigenvalues of the diagonal blocks, the result follows. Corollary 1 is evident from the identity $|\mathbf{A}| = \Pi_{l=1}^{QR}\lambda(l)$. □

Details on the existence and structure of $\mathbf{U}$ can be found in [13]. Also, it is possible to rearrange the elements of $\mathbf{A}$ such that it is circulant at the block level, with each $\mathbf{A}_{ij}$ an arbitrary matrix. A method for calculating the eigenvalues of such a matrix is given in [14].

Taking $\mathbf{A} = \mathbf{B}(\boldsymbol{\theta})$ in Theorem 1, it is apparent that the eigenvalues of $\mathbf{B}(\boldsymbol{\theta})$ are equal to the eigenvalues of

$$\Lambda(\mathbf{t}) = \begin{bmatrix} \lambda_{11}(\mathbf{t}) & \lambda_{12}(\mathbf{t}) & \cdots & \lambda_{1P}(\mathbf{t}) \\ \lambda_{21}(\mathbf{t}) & \lambda_{22}(\mathbf{t}) & \cdots & \lambda_{2P}(\mathbf{t}) \\ \vdots & \vdots & \ddots & \vdots \\ \lambda_{P1}(\mathbf{t}) & \lambda_{P2}(\mathbf{t}) & \cdots & \lambda_{PP}(\mathbf{t}) \end{bmatrix}, \ \forall \mathbf{t} \in \Omega \tag{20}$$

where the eigenvalues of the submatrices $\mathbf{B}(\boldsymbol{\theta}_{ij})$ are given by [11]:

$$\lambda_{ij}(\mathbf{t}) = \delta_{ij} - \sum_{\mathbf{r}\in N_{ij}} \theta_{ij}(\mathbf{r}) e^{\sqrt{-1}\omega_{\mathbf{rt}}}, \ \omega_{\mathbf{rt}} = \frac{2\pi(km+ln)}{M}$$
$$\text{for } \mathbf{r} = (k,l) \text{ and } \mathbf{t} = (m,n) \tag{21}$$

From Corollary 1, $|\mathbf{B}(\boldsymbol{\theta})| = \Pi_{\mathbf{t}\in\Omega}|\Lambda(\mathbf{t})|$. Therefore, (17) can be written as

$$\left|\Sigma_{\mathbf{y}}^{-1}\right| = \left(\prod_{i=1}^{P}\rho_i\right)^{-M^2}\left(\prod_{\mathbf{t}\in\Omega}|\Lambda(\mathbf{t})|\right)^2. \tag{22}$$

Substituting (16) and (22) into (10), the ML objective function for the MSAR model simplifies to

$$J(\boldsymbol{\theta},\boldsymbol{\rho}) = \sum_{i=1}^{P}\frac{1}{\rho_i}\sum_{\mathbf{s}\in\Omega}\left(y_i(\mathbf{s}) - \sum_{j=1}^{P}\sum_{\mathbf{r}\in N_{ij}}\theta_{ij}(\mathbf{r})y_j(\mathbf{s}\oplus\mathbf{r})\right)^2 + M^2\sum_{i=1}^{P}\log\rho_i - 2\sum_{\mathbf{t}\in\Omega}\log|\Lambda(\mathbf{t})| \tag{23}$$

Differentiating (23) with respect to each of the ρ_i and equating to zero, the ML estimates of the noise variances are obtained as

$$\hat{\rho}_i = \frac{1}{M^2}\sum_{\mathbf{s}\in\Omega}\left(y_i(\mathbf{s}) - \sum_{j=1}^{P}\sum_{\mathbf{r}\in N_{ij}}\theta_{ij}(\mathbf{r})y_j(\mathbf{s}\oplus\mathbf{r})\right)^2. \tag{24}$$

Substituting $\rho_i = \hat{\rho}_i$ into (23) and eliminating constant terms, the MSAR ML objective function reduces to

$$\tilde{J}(\theta) = M^2\sum_{i=1}^{P}\log\left(\sum_{\mathbf{s}\in\Omega}\left(y_i(\mathbf{s}) - \sum_{j=1}^{P}\sum_{\mathbf{r}\in N_{ij}}\theta_{ij}(\mathbf{r})y_j(\mathbf{s}\oplus\mathbf{r})\right)^2\right) - 2\sum_{\mathbf{t}\in\Omega}\log|\Lambda(\mathbf{t})| \tag{25}$$

The ML estimates for the neighbor coefficients are obtained by choosing $\boldsymbol{\theta}$ such that (25) is minimized. Standard numerical methods for nonlinear optimization may be used for this task. Minimization of (25) is usually accomplished using a derivative based technique, where

$$\frac{\partial\tilde{J}(\boldsymbol{\theta})}{\partial\theta_{pq}(\mathbf{h})} = -2M^2\frac{\sum_{\mathbf{s}\in\Omega}\left(y_p(\mathbf{s}) - \sum_{j=1}^{P}\sum_{\mathbf{r}\in N_{pj}}\theta_{pj}(\mathbf{r})y_j(\mathbf{s}\oplus\mathbf{r})\right)y_q(\mathbf{s}\oplus\mathbf{h})}{\sum_{\mathbf{s}\in\Omega}\left(y_p(\mathbf{s}) - \sum_{j=1}^{P}\sum_{\mathbf{r}\in N_{pj}}\theta_{pj}(\mathbf{r})y_j(\mathbf{s}\oplus\mathbf{r})\right)^2} + 2\sum_{\mathbf{t}\in\Omega}\frac{\left|\Lambda(\mathbf{t})_{pq}\right|e^{\sqrt{-1}\omega_{\mathbf{ht}}}}{|\Lambda(\mathbf{t})|} \tag{26}$$

and $|\Lambda(\mathbf{t})_{pq}|$ is the cofactor of $\lambda_{pq}(\mathbf{t})$.

Finally, it should be noted that the arguments of the second term summation in (25) and (26) are, in general, complex. However, these arguments occur in complex conjugate pairs and the resultant summation is real. Furthermore, this Hermitian symmetry can be exploited to substantially reduce the required computations.

3 MULTISPECTRAL MARKOV RANDOM FIELD (MMRF) MODELS

A multispectral image may be considered Markovian with respect to its neighbor set if it has the property

$$p(y_i(\mathbf{s}) \mid \text{all other image observations}) = p(y_i(\mathbf{s}) \mid \text{neighborhood observations}). \tag{27}$$

Because the conditional distributions of $y_i(\mathbf{s})$ given all other observations and $y_i(\mathbf{s})$ given only the neighborhood observations are the same, the *best linear estimator* of the observed values may be written in terms of the neighborhood observations as

$$y_i(\mathbf{s}) = \sum_{j=1}^{P}\sum_{\mathbf{r}\in N_{ij}}\theta_{ij}(\mathbf{r})y_j(\mathbf{s}\oplus\mathbf{r}) + e_i(\mathbf{s}), \ \mathbf{s}\in\Omega \text{ and } i = 1, \ldots, P \tag{28}$$

where the θ_{ij}s are taken as the coefficients of the minimum-mean-square-error (MMSE) estimate of $y_i(\mathbf{s})$, and $e_i(\mathbf{s})$ denotes the estimation error. This result holds as a direct consequence of the Markov assumption (27). Due to the MMSE assumption, the estimation errors have a orthogonality property given by

$$E\{y_i(\mathbf{s})e_j(\mathbf{r})\} = \begin{cases}\rho_i & i = j \text{ and } \mathbf{s} = \mathbf{r} \\ 0 & \text{otherwise}\end{cases} \tag{29}$$

where ρ_i is the variance of the estimation error (noise) sequence, $\{e_i(\mathbf{s})\}$.

In matrix form, (28) can be written as

$$\mathbf{B}(\boldsymbol{\theta})\mathbf{y} = \mathbf{e}, \tag{30}$$

where $\mathbf{B}(\boldsymbol{\theta})$,$\mathbf{y}$, and $\mathbf{e}$ are defined in the same manner as their MSAR counterparts (2). Similarly, the orthogonal property of the MMSE estimates can be expressed as

$$E\{\mathbf{y}\mathbf{e}^T\} = \begin{bmatrix} \rho_1\mathbf{I} & \mathbf{0} & \cdots & \mathbf{0} \\ \mathbf{0} & \rho_2\mathbf{I} & \cdots & \mathbf{0} \\ \vdots & \vdots & \ddots & \vdots \\ \mathbf{0} & \mathbf{0} & \cdots & \rho_P\mathbf{I} \end{bmatrix} = \Sigma_{\mathbf{w}}. \quad (31)$$

Using (30) and (31), the correlation structure of the estimation error sequences $\{e_i(\mathbf{s})\}$ can be written as

$$\Sigma_{\mathbf{e}} = E\{\mathbf{e}\mathbf{e}^T\} = E\{\mathbf{B}(\boldsymbol{\theta})\mathbf{y}\mathbf{e}^T\} = \mathbf{B}(\boldsymbol{\theta})E\{\mathbf{y}\mathbf{e}^T\} = \mathbf{B}(\boldsymbol{\theta})\Sigma_{\mathbf{w}}. \quad (32)$$

The MMRF model parameters $\boldsymbol{\rho}$ and $\boldsymbol{\theta}$ must be chosen such that $\Sigma_{\mathbf{e}}$ is positive definite. From (32), it is apparent that the the stationary noise sequences $\{e_i(\mathbf{s})\}$ have the correlation structure

$$v_{ij}(\mathbf{r}) = E\{e_i(\mathbf{s})e_j(\mathbf{s}\oplus\mathbf{r})\} = \begin{cases} -\theta_{ij}(\mathbf{r})\rho_j & \mathbf{r}\in N_{ij} \\ \rho_j & \mathbf{r} = 0 \text{ and } i = j \\ 0 & \text{otherwise} \end{cases} \quad (33)$$

The correlation functions $v_{ij}(\mathbf{r})$ have a symmetry property which must be considered with respect to the model parameters. Note that, because the noise sequences are stationary, these correlation functions must satisfy

$$v_{ij}(\mathbf{r}) = E\{e_i(\mathbf{s})e_j(\mathbf{s}\oplus\mathbf{r})\} = E\{e_i(\mathbf{s}\oplus -\mathbf{r})e_j(\mathbf{s})\} = v_{ji}(-\mathbf{r}). \quad (34)$$

Taken together, (33) and (34) implicitly impose a symmetry constraint on the MMRF neighbor sets and their associated coefficients, i.e.,

$$v_{ij}(\mathbf{r}) = v_{ji}(-\mathbf{r}) \Rightarrow -\theta_{ij}(\mathbf{r})\rho_j = -\theta_{ji}(-\mathbf{r})\rho_i$$

which leads to the conclusion that

$$\mathbf{r}\in N_{ij} \Leftrightarrow -\mathbf{r}\in N_{ji} \text{ and } \rho_j\theta_{ij}(\mathbf{r}) = \rho_i\theta_{ji}(-\mathbf{r}). \quad (35)$$

Note that intraplane neighbor sets, N_{ii}, must be self-symmetric and may be specified by an asymmetric half-plane neighbor set. Interplane neighbor sets, $N_{ij,i\neq j}$, can be arbitrarily defined in pairs as required by the given symmetry property. An equivalent statement of the MMRF symmetry constraint is that a valid model must have $\rho_j\mathbf{B}(\boldsymbol{\theta}_{ij}) = \rho_i\mathbf{B}(\boldsymbol{\theta}_{ji})^T$.

Using (30) and (32), the covariance matrix of the image observations can be expressed as

$$\Sigma_{\mathbf{y}} = E\{\mathbf{y}\mathbf{y}^T\} = E\left\{\mathbf{B}(\boldsymbol{\theta})^{-1}\mathbf{e}\mathbf{e}^T\left[\mathbf{B}(\boldsymbol{\theta})^{-1}\right]^T\right\} = \mathbf{B}(\boldsymbol{\theta})^{-1}\Sigma_{\mathbf{e}}\left[\mathbf{B}(\boldsymbol{\theta})^{-1}\right]^T = \mathbf{B}(\boldsymbol{\theta})^{-1}\Sigma_{\mathbf{w}} \quad (36)$$

To be admissible as a covariance matrix, the model parameters $\boldsymbol{\rho}$ and $\boldsymbol{\theta}$ must be chosen such that $\Sigma_{\mathbf{y}}$ is positive definite. This is consistent with the requirement that $\Sigma_{\mathbf{e}}$ be positive definite, since $\Sigma_{\mathbf{y}} = \Sigma_{\mathbf{w}}\Sigma_{\mathbf{e}}^{-1}\Sigma_{\mathbf{w}}$.

Further details of the MMRF model, including methods for image synthesis and least squares estimation of model parameters, can be found in [10], [12].

3.1 Maximum Likelihood Estimation of MMRF Model Parameters

If it is assumed that an observed image $\{\mathbf{y}(\mathbf{s})\}$ is a realization of a MMRF model having a multivariate Gaussian distribution, then the MMRF log-likelihood function is given by (9) and the maximum likelihood estimates are obtained as the parameter values for which (10) is minimized. For the MMRF model, the image covariance matrix inverse is given by $\Sigma_{\mathbf{y}}^{-1} = \Sigma_{\mathbf{w}}^{-1}\mathbf{B}(\theta)$ and the quadratic portion of (10) can be written as

$$\mathbf{y}^T\Sigma_{\mathbf{y}}^{-1}\mathbf{y} = \sum_{i=1}^{P}\sum_{j=1}^{P}\frac{1}{\rho_i}\mathbf{y}_i^T\mathbf{B}(\boldsymbol{\theta}_{ij})\mathbf{y}_j. \quad (37)$$

Using the identity $\mathbf{x}^T\mathbf{A}\mathbf{x} = \text{tr}\{\mathbf{A}\mathbf{x}\mathbf{x}^T\}$ and exploiting the block-circulant structure of $\mathbf{B}(\boldsymbol{\theta}_{ij})$ yields

$$\mathbf{y}_i^T\mathbf{B}(\boldsymbol{\theta}_{ij})\mathbf{y}_j = \begin{cases} \sum_{\mathbf{s}\in\Omega} y_i(\mathbf{s})^2 - 2\sum_{\mathbf{r}\in N_{ii}}\theta_{ii}(\mathbf{r})\sum_{\mathbf{s}\in\Omega} y_i(\mathbf{s})y_i(\mathbf{s}\oplus\mathbf{r}) & i = j \\ -\sum_{\mathbf{r}\in N_{ij}}\theta_{ij}(\mathbf{r})\sum_{\mathbf{s}\in\Omega} y_i(\mathbf{s})y_j(\mathbf{s}\oplus\mathbf{r}) & i \neq j \end{cases} \quad (38)$$

where the intraplane neighborhoods, N_{ii}, are specified in terms of asymmetic half-plane neighbor sets. Defining

$$u_i = \frac{1}{\rho_i},$$

$$P_{ij}(\mathbf{r}) = \frac{1}{\rho_i}\theta_{ij}(\mathbf{r}),$$

and

$$R_{ij}(\mathbf{r}) = \sum_{\mathbf{s}\in\Omega} y_i(\mathbf{s})y_j(\mathbf{s}\oplus\mathbf{r})$$

and substituting (38) into (37), the quadratic term reduces to

$$\mathbf{y}^T\Sigma_{\mathbf{y}}^{-1}\mathbf{y} = \sum_{i=1}^{P}\sum_{j=1}^{P}\left(\delta_{ij}u_iR_{ii}(\mathbf{0}) - \left(1+\delta_{ij}\right)\sum_{\mathbf{r}\in N_{ij}}P_{ij}(\mathbf{r})R_{ij}(\mathbf{r})\right) = \sum_{i=1}^{P}u_iR_{ii}(\mathbf{0}) - \sum_{i=1}^{P}\sum_{j=1}^{P}\left(1+\delta_{ij}\right)\sum_{\mathbf{r}\in N_{ij}}P_{ij}(\mathbf{r})R_{ij}(\mathbf{r}) \quad (39)$$

From symmetry properties of the MMRF model, i.e.,

$$\mathbf{r}\in N_{ij} \Leftrightarrow -\mathbf{r}\in N_{ji},$$

$$P_{ij}(\mathbf{r}) = P_{ji}(-\mathbf{r}),$$

and

$$R_{ij}(\mathbf{r}) = R_{ji}(-\mathbf{r}),$$

it is evident that

$$\sum_{\mathbf{r}\in N_{ij}}P_{ij}(\mathbf{r})R_{ij}(\mathbf{r}) = \sum_{\mathbf{r}\in N_{ji}}P_{ji}(\mathbf{r})R_{ji}(\mathbf{r}) \quad (40)$$

and (39) is further simplified as

$$\mathbf{y}^T\Sigma_{\mathbf{y}}^{-1}\mathbf{y} = \sum_{i=1}^{P}u_iR_{ii}(\mathbf{0}) - 2\sum_{i=1}^{P}\sum_{j=i}^{P}\sum_{\mathbf{r}\in N_{ij}}P_{ij}(\mathbf{r})R_{ij}(\mathbf{r}). \quad (41)$$

By application of Theorem 1 and its corollary, the determinant in (10) can also be simplified as

$$\left|\Sigma_{\mathbf{y}}^{-1}\right| = \left|\Sigma_{\mathbf{w}}^{-1}\right|\left|\mathbf{B}(\theta)\right| = \left|\Sigma^{-1}\right|^{M^2}\prod_{\mathbf{t}\in\Omega}\left|\Lambda(\mathbf{t})\right| = \prod_{\mathbf{t}\in\Omega}\left|\Sigma^{-1}\right|\left|\Lambda(\mathbf{t})\right| = \prod_{\mathbf{t}\in\Omega}\left|\Sigma^{-1}\Lambda(\mathbf{t})\right| = \prod_{\mathbf{t}\in\Omega}\left|\mathbf{L}(\mathbf{t})\right| \quad (42)$$

where $\mathbf{L}(\mathbf{t}) = \Sigma^{-1}\Lambda(\mathbf{t})$, $\Sigma = \text{diag}\{\rho_i,\ i = 1, \ldots, P\}$, and $\Lambda(\mathbf{t})$ is given by (20). The (i, j)th element of $\mathbf{L}(\mathbf{t})$ is given by

$$l_{ij}(\mathbf{t}) = \frac{1}{\rho_i}\lambda_{ij}(\mathbf{t}) = \begin{cases} u_i - 2\sum_{\mathbf{r}\in N_{ii}}P_{ii}(\mathbf{r})\cos\omega_{\mathbf{rt}} & i = j \\ -\sum_{\mathbf{r}\in N_{ij}}P_{ij}(\mathbf{r})e^{\sqrt{-1}\omega_{\mathbf{rt}}} & i \neq j \end{cases} \quad (43)$$

Note that, due to the symmetry property of the MMRF neighbor coefficients, $\lambda_{ij}(\mathbf{t})$ is real-valued when $i = j$. The model symmetry also ensures that $\mathbf{L}(\mathbf{t})$ is Hermitian and therefore $|\mathbf{L}(\mathbf{t})|$ is real val-

TABLE 1
MULTISPECTRAL MODEL PARAMETER ESTIMATION RESULTS

MSAR Model

Model Parameter	True value	LS Est.	ML Est.
ρ_r	1.6939	1.2881	1.6740
θ_{rr}(1, 0)	0.1807	0.1688	0.1756
(0, 1)	0.2419	0.1184	0.2289
(-1, 0)	0.0215	0.0252	0.0212
(0,-1)	0.0682	0.0389	0.0671
θ_{rg}(0, 0)	0.7446	0.8314	0.7321
(1, 0)	-0.1403	-0.1556	-0.1334
(0, 1)	-0.1517	-0.1192	-0.1393
θ_{rb}(0, 0)	0.0816	0.0634	0.0956
(1, 0)	-0.0260	-0.0045	-0.0278
(0, 1)	-0.0412	-0.0050	-0.0438
ρ_g	1.6463	1.0590	1.6680
θ_{gr}(0, 0)	0.7268	0.7989	0.7222
(-1, 0)	-0.1448	-0.1169	-0.1458
(0,-1)	-0.1811	-0.1934	-0.1848
θ_{gg}(1, 0)	0.0419	0.0137	0.0409
(0, 1)	0.1304	0.1159	0.1304
(-1, 0)	0.1075	0.0806	0.1086
(0,-1)	0.1953	0.1672	0.1993
θ_{gb}(0, 0)	0.2034	0.2120	0.2067
(1, 0)	-0.0319	-0.0086	-0.0311
(0, 1)	-0.0584	-0.0807	-0.0586
ρ_b	5.7882	5.1490	5.8694
θ_{br}(0, 0)	0.2963	0.1127	0.2576
(-1, 0)	-0.1044	-0.1262	-0.1113
(0,-1)	-0.1579	-0.1030	-0.1501
θ_{bg}(0, 0)	0.6797	0.9282	0.7114
(-1, 0)	-0.0491	-0.0580	-0.0451
(0,-1)	-0.1332	-0.2868	-0.1390
θ_{bb}(1, 0)	-0.0005	-0.0019	-0.0006
(0, 1)	0.1027	0.0635	0.1036
(-1, 0)	0.1522	0.1799	0.1550
(0,-1)	0.3234	0.3824	0.3250

MMRF Model

Model Parameter	True value	LS Est.	ML Est.
ρ_r	310.19	311.16	310.90
θ_{rr}(1, 0), (-1, 0)	0.2637	0.2617	0.2585
(0, 1), (0,-1)	0.3016	0.2983	0.3002
(1, 1), (-1,-1)	-0.0849	-0.0906	-0.0920
(1,-1), (-1, 1)	-0.0324	-0.0264	-0.0254
(2, 0), (-2, 0)	-0.0393	-0.0420	-0.0399
(0, 2), (0,-2)	-0.0480	-0.0450	-0.0444
θ_{rg}(0, 0)	0.3099	0.2994	0.3068
(1, 0)	-0.1474	-0.1405	-0.1447
(0, 1)	-0.2155	-0.2170	-0.2180
(-1, 0)	0.1286	0.1272	0.1312
(0,-1)	-0.0624	-0.0710	-0.0699
θ_{rb}(0, 0)	-0.0449	-0.0334	-0.0388
(1, 0)	0.0490	0.0358	0.0376
(0, 1)	0.0524	0.0471	0.0521
(-1, 0)	-0.0516	-0.0457	-0.0498
(0,-1)	-0.0031	-0.0052	-0.0029
ρ_g	189.35	191.68	191.09
θ_{gr}(0, 0)	0.1892	0.1845	0.1886
(-1, 0)	-0.0900	-0.0865	-0.0889
(0,-1)	-0.1316	-0.1336	-0.1340
(-1,-1)	0.0785	0.0784	0.0806
(-1, 1)	-0.0381	-0.0437	-0.0429
θ_{gg}(1, 0), (-1, 0)	0.2415	0.2372	0.2348
(0, 1), (0,-1)	0.2893	0.2929	0.2925
(1, 1), (-1,-1)	-0.1227	-0.1092	-0.1127
(1,-1), (-1, 1)	0.0053	0.0048	0.0070
(2, 0), (-2, 0)	-0.0293	-0.0363	-0.0340
(0, 2), (0,-2)	-0.0303	-0.0413	-0.0365
θ_{gb}(0, 0)	0.2396	0.2375	0.2402
(1, 0)	-0.0833	-0.0801	-0.0802
(0, 1)	-0.1625	-0.1593	-0.1607
(-1, 0)	0.0918	0.0893	0.0917
(0,-1)	-0.0681	-0.0687	-0.0701
ρ_b	304.72	306.95	306.55
θ_{br}(0, 0)	-0.0441	-0.0329	-0.0383
(-1, 0)	0.0482	0.0354	0.0371
(0,-1)	0.0515	0.0465	0.0514
(-1,-1)	-0.0507	-0.0451	-0.0491
(-1, 1)	-0.0031	-0.0051	-0.0029
θ_{bg}(0, 0)	0.3856	0.3803	0.3853
(-1, 0)	-0.1340	-0.1283	-0.1287
(0,-1)	-0.2616	-0.2551	-0.2578
(-1,-1)	0.1478	0.1430	0.1471
(-1, 1)	-0.1096	-0.1100	-0.1124
θ_{bb}(1, 0), (-1, 0)	0.2450	0.2458	0.2442
(0, 1), (0,-1)	0.2883	0.2852	0.2862
(1, 1), (-1,-1)	-0.1024	-0.1027	-0.1058
(1,-1), (-1, 1)	-0.0036	0.0024	0.0028
(2, 0), (-2, 0)	-0.0372	-0.0444	-0.0420
(0, 2), (0,-2)	-0.0346	-0.0285	-0.0287

ued $\forall \mathbf{t} \in \Omega$. Furthermore, from Theorem 1, it is evident that for a valid MMRF model, $\mathbf{L(t)}$ will be positive definite $\forall \mathbf{t} \in \Omega$.

Substituting (41) and (42) into (10), the MMRF objective function becomes

$$J(\mathbf{P},\mathbf{u}) = \mathbf{y}^T\Sigma_{\mathbf{y}}^{-1}\mathbf{y} - \log\left|\Sigma_{\mathbf{y}}^{-1}\right| = \sum_{i=1}^{P} u_i R_{ii}(\mathbf{0}) - 2\sum_{i=1}^{P}\sum_{j=1}^{P}\sum_{\mathbf{r}\in N_{ij}} P_{ij}(\mathbf{r})R_{ij}(\mathbf{r}) - \sum_{\mathbf{t}\in\Omega}\log\left|\mathbf{L(t)}\right| \quad (44)$$

From $\hat{\mathbf{P}}$ and $\hat{\mathbf{u}}$ which minimizes (44) MMRF model estimates are obtained as $\rho_i = \frac{1}{u_i}$ and $\theta_{ij}(\mathbf{r}) = \rho_i P_{ij}(\mathbf{r})$. As before, standard methods for nonlinear optimization are used in the minimization procedure. For the MMRF model, the derivatives of (44) with respect to each unknown parameter are given by

$$\frac{\partial J(\mathbf{P},\mathbf{u})}{\partial u_p} = R_{pp}(\mathbf{0}) - \sum_{\mathbf{t}\in\Omega}\frac{\left|\mathbf{L(t)}_{pp}\right|}{\left|\mathbf{L(t)}\right|} \quad (45)$$

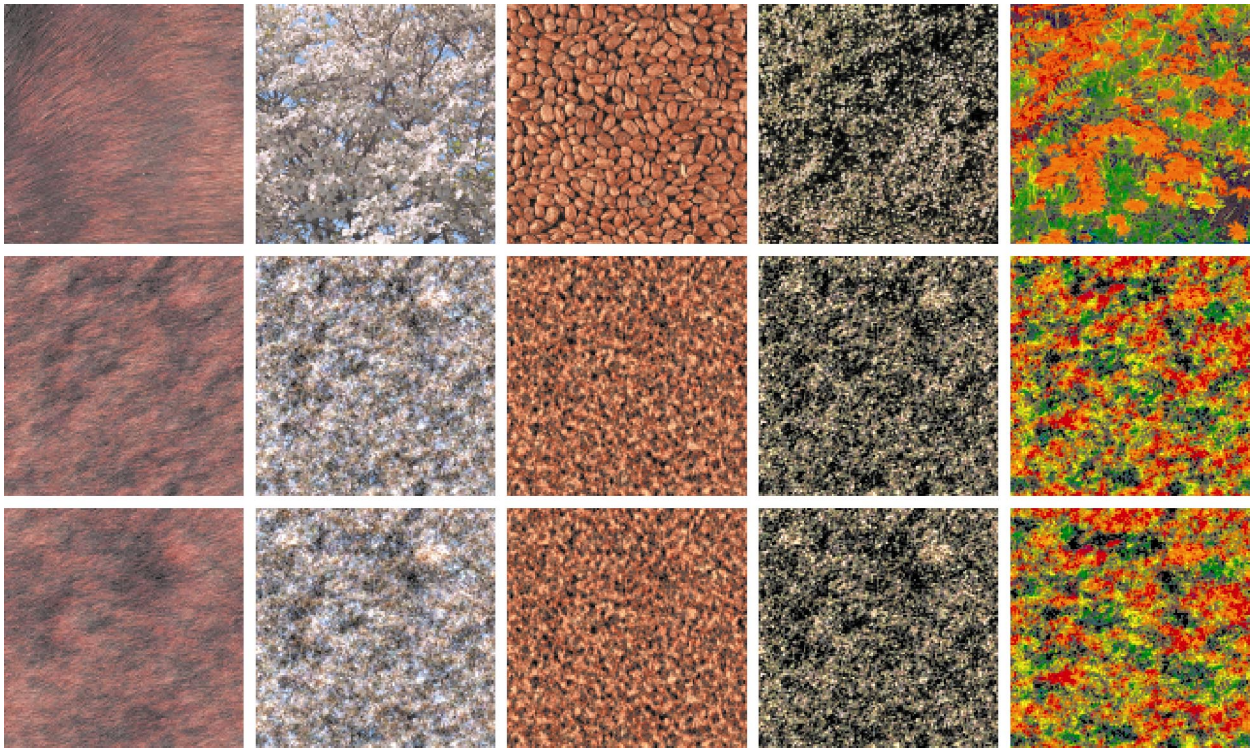

Fig. 1. Color RF model image synthesis. Original images are shown on the top row. Images synthesized from the MSAR and MMRF model ML parameter estimates are shown in the center and bottom rows, respectively.

$$\frac{\partial J(\mathbf{P},\mathbf{u})}{\partial P_{pq}(\mathbf{h})} = \begin{cases} 2\left(\sum_{\mathbf{t}\in\Omega} \frac{\left|\mathbf{L}(\mathbf{t})_{pp}\right| \cos \omega_{\mathbf{ht}}}{|\mathbf{L}(\mathbf{t})|} - R_{pp}(\mathbf{h})\right) & p = q \\ 2\left(\sum_{\mathbf{t}\in\Omega} \frac{\left|\mathbf{L}(\mathbf{t})_{pq}\right| e^{\sqrt{-1}\omega_{\mathbf{ht}}}}{|\mathbf{L}(\mathbf{t})|} - R_{pq}(\mathbf{h})\right) & p \neq q \end{cases} \quad (46)$$

where $|\mathbf{L}(\mathbf{t})_{pq}|$ is the cofactor of $l_{pq}(\mathbf{t})$. As for the MSAR model, symmetry of $\mathbf{L}(\mathbf{t})$ ensures that (45) and (46) are real valued and can be exploited to reduce the required computations.

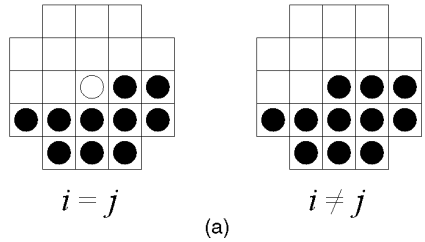

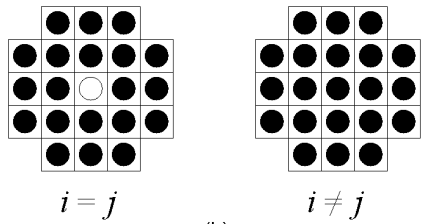

Fig. 2. Neighbor sets, N_{ij}, used for modeling color texture images. The (0, 0) position is represented by ∘, and • denotes the relative neighbor locations. (a) Nonsymmetric neighborhood. (b) Symmetric neighborhood.

The procedure for minimizing (44) must be subject to the constraint that $\mathbf{L}(\mathbf{t})$ remain positive definite $\forall \mathbf{t} \in \Omega$. This is consistent with the requirement that $\Sigma_{\mathbf{e}}$ in (32) and $\Sigma_{\mathbf{y}}$ in (36) be positive definite.

4 Experimental Results

A series of experiments were conducted to study the characteristics of the proposed MSAR and MMRF ML estimation procedures. The RGB color model was assumed, i.e., $P = 3$ and $i, j \in \{r, g, b\}$, and images with dimension 128×128 were used in all experiments. The nonlinear optimization method used to minimize the given ML objective functions in these experiments was the Fletcher-Reeves conjugate gradient method [15]. The least squares (LS) estimates given in [9], [10] were taken as the initial condition for the optimization procedure. Experiments using the zero vector as an initial condition indicate that this choice has little effect on the end result, however, starting with a reasonable estimate can substantially reduce the required number of iterations in the optimization process. The rate of convergence is determined primarily by the condition number of the image covariance matrix $\Sigma_{\mathbf{y}}$.

In the first series of experiments, the effectiveness of the ML estimation procedures was evaluated. Synthetic images were generated from known models using the methods given in [9], [10], and the ML parameter estimates were calculated from these image samples. In all cases, these estimates were very close to the true parameter values. The results given in Table 1 are typical of these experiments. When compared to LS estimates, the ML method consistently produced superior results. The degree of improvement was most pronounced for the MSAR models. It should also be noted that the ML estimation method implemented in this work ensures that the resultant model will satisfy the MMRF validity constraints given in Section 3, whereas the LS estimates often produce models which do not. In applications requiring synthetic generation of MMRF images, this alone can justify the additional computational burden of the ML method.

A second series of experiments was conducted to evaluate the ability of these models to characterize natural texture samples. This involved estimating color SAR and MRF parameters from a set of natural color texture samples [16] and synthesizing images from the estimated parameters. The synthetic images were then visually compared to the original images. In most cases, the synthetic images are observed to be quite similar in appearance to the original images from which the models were derived. Fig. 1 gives examples of these experiments. For the nonsymmetric color SAR models, the neighbor sets used in these experiments are given in Fig. 2a, and the corresponding neighbor sets for the symmetric color SAR and MRF models are shown in Fig. 2b.

5 Conclusions

In this work, we provide the analytical basis for obtaining ML parameter estimates of multispectral RF image models. Objective functions were derived which are computationally efficient and, when minimized, produce true ML parameter estimates for the MSAR and MMRF image models. Experimental results based on images generated from known models demonstrate the effectiveness of the ML estimation methods. Further experiments using natural texture samples show that MSAR and MMRF models using ML estimates are effective at capturing the principal characteristics of color texture images.

References

[1] A. Gagalowicz, S.D. Ma, and C. Tournier-Lasserve, "Efficient Models for Color Textures," *Proc. Int'l Conf. Pattern Recognition*, pp. 412–414, Paris, Oct. 1986.

[2] R.L. Kashyap and R. Chellappa, "Estimation and Choice of Neighbors in Spatial-Interaction Models of Images," *IEEE Trans. Information Theory*, vol. 29, no. 1, pp. 60–72, Jan. 1983.

[3] A. Khotanzad and R.L. Kashyap, "Feature Selection for Texture Recognition Based on Image Synthesis," *IEEE Trans. Systems, Man, and Cybernetics*, vol. 17, no. 6, pp. 1,087–1,095, Nov./Dec. 1987.

[4] R. Chellappa, S. Chatterjee, and R. Bagdazian, "Texture Synthesis and Compression Using Gaussian-Markov Random Field Models," *IEEE Trans. Systems, Man, and Cybernetics*, vol. 15, no. 2, pp. 298–303, Mar./Apr. 1985.

[5] W.E. Larimore, "Statistical Inference on Stationary Random Fields," *Proc. IEEE*, vol. 65, pp. 961–970, June 1977.

[6] J.E. Besag, "Spatial Interaction and Statistical Analysis of Lattice Systems," *J. Royal Statistical Soc., Series B*, vol. B36, pp. 192–236, 1974.

[7] P. Whittle, "On Stationary Processes in the Plane," *Biometrika*, vol. 41, pp. 434–449, 1954.

[8] D.K. Panjwani and G. Healey, "Markov Random Field Models for Unsupervised Segmentation of Textured Color Images," *IEEE Trans. Pattern Analysis and Machine Intelligence*, vol. 17, no. 10, pp. 939–954, Oct. 1995.

[9] J. Bennett and A. Khotanzad, "Multispectral and Color Image Modeling and Synthesis Using Random Field Models," *Proc. IEEE Int'l Conf. Image Processing*, vol. 3, pp. 991–994, Lausanne, Switzerland, Sept. 1996.

[10] J. Bennett and A. Khotanzad, "Multispectral Random Field Models for Synthesis and Analysis of Color Images," *IEEE Trans. Pattern Analysis and Machine Intelligence*, vol. 20, no. 3, pp. 327–332, Mar. 1998.

[11] R.L. Kashyap, "Random Field Models on Torus Lattices for Finite Images," *Proc. Int'l Conf. Pattern Recognition*, pp. 1,103–1,105, Miami, Fla., Dec. 1980.

[12] J.W. Bennett, "Modeling and Analysis of Gray Tone, Color, and Multispectral Texture Images by Random Field Models and Their Generalizations," PhD dissertation, Electrical Eng. Dept., Southern Methodist Univ., Dallas, Texas, May 1997.

[13] R.C. Gonzalez and R.E. Woods, *Digital Image Processing*, chapter 5, pp. 261–268. Reading, Mass.: Addison-Wesley, 1992.

[14] A.K. Katsaggelos, K.T. Lay, and N.P. Galatsanos, "A General Framework for Frequency Domain Multi-Channel Signal Processing," *IEEE Trans. Image Processing*, vol. 2, no. 3, pp. 417–420, July 1993.

[15] D.A.H. Jacobs, ed., *The State of the Art in Numerical Analysis*, chapter 3. London: Academic Press, 1977.

[16] Vision and Modeling Group, MIT Media Laboratory, "Vision Texture (VisTex) Database," http://www-white.media.mit.edu/vismod/, 1995.